

# Index Network

Hao Lu, Yutong Dai, Chunhua Shen, Songcen Xu

**Abstract**—We show that existing upsampling operators can be unified using the notion of the index function. This notion is inspired by an observation in the decoding process of deep image matting where indices-guided unpooling can often recover boundary details considerably better than other upsampling operators such as bilinear interpolation. By viewing the indices as a function of the feature map, we introduce the concept of ‘learning to index’, and present a novel index-guided encoder-decoder framework where indices are self-learned adaptively from data and are used to guide the downsampling and upsampling stages, without extra training supervision. At the core of this framework is a new learnable module, termed Index Network (IndexNet), which dynamically generates indices conditioned on the feature map itself. IndexNet can be used as a plug-in applying to almost all off-the-shelf convolutional networks that have coupled downsampling and upsampling stages, giving the networks the ability to dynamically capture variations of local patterns. In particular, we instantiate and investigate five families of IndexNet and demonstrate their effectiveness on four dense prediction tasks, including image denoising, image matting, semantic segmentation, and monocular depth estimation. Code and models have been made available at: <https://tinyurl.com/IndexNetV1>

**Index Terms**—Index Networks, Upsampling Operators, Image Denoising, Semantic Segmentation, Image Matting, Monocular Depth Estimation.



## 1 INTRODUCTION

UPSAMPLING is an essential stage for dense prediction tasks using deep convolutional neural networks (CNNs). The frequently used upsampling operators include transposed convolution [1], [2], unpooling [3], *periodic shuffling* [4] (also known as depth-to-space), and naive interpolation [5], [6] followed by convolution. These operators, however, are not general-purpose designs and often exhibit different behaviors in different tasks.

The widely-adopted upsampling operator in semantic segmentation and depth estimation is bilinear interpolation, while unpooling is less popular. A reason might be that the feature map generated by max unpooling is very sparse, while the bilinearly interpolated feature map has dense and consistent representations for local regions (compared to the feature map before interpolation). This is particularly beneficial for semantic segmentation and depth estimation where pixels in a region often share the same class label or have similar depth. However, we observe that bilinear interpolation can perform significantly worse than unpooling in boundary-sensitive tasks such as image matting. A fact is that the leading deep image matting model [7] largely borrows the design from the SegNet [3], where unpooling was first introduced. When adapting other state-of-the-art segmentation models, such as DeepLabv3+ [6] and RefineNet [5], to this task, unfortunately, we observe both DeepLabv3+ and RefineNet fail to recover boundary details (Fig. 1), compared to SegNet. A plausible explanation is that, compared to the bilinearly upsampled feature map, unpooling uses max-pooling indices to guide upsampling. Since boundaries in the shallow layers usually have the maximum responses, indices extracted from these responses

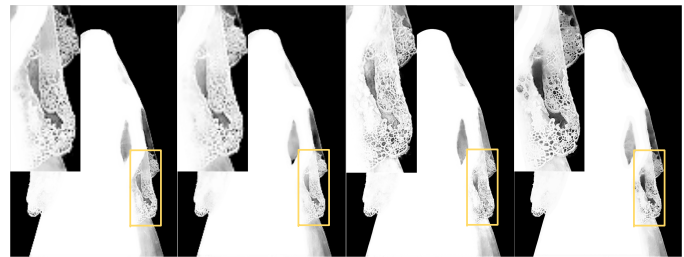


Fig. 1. Alpha mattes of different models for the task of image matting. From left to right, DeepLabv3+ [6], RefineNet [5], DeepMatting [7] and IndexNet (Ours). Bilinear upsampling fails to recover subtle details, while unpooling and our learned upsampling operator can produce much clear mattes with good local contrast.

record the boundary locations. The feature map projected by the indices thus shows improved boundary delineation.

Analyses above reveal a fact that, different upsampling operators have different characteristics, and we expect a specific behavior of the upsampling operator when dealing with specific image content for a certain vision task. A question of interest is: *Can we design a generic operator to upsample feature maps that better predict boundaries and regions simultaneously?* A key observation of this work here is that unpooling, bilinear interpolation or other *upsampling operators are some forms of index functions*. For example, the nearest neighbor interpolation of a point is equivalent to allocating indices of one to its neighbor and then map the value of the point. In this sense, indices are models [8], therefore indices can be modeled and learned.

In this work, *we model indices as a function of the local feature map and learn index functions to perform upsampling within deep CNNs*. In particular, we present a novel index-guided encoder-decoder framework, which naturally generalizes models like SegNet. Instead of using max-pooling and unpooling, we introduce indexed pooling and indexed up-

- H. Lu, Y. Dai and C. Shen are with The University of Adelaide, SA 5005, Australia. Corresponding author: C. Shen.  
E-mail: [firstname.lastname@adelaide.edu.au](mailto:firstname.lastname@adelaide.edu.au).
- S. Xu is with Noah’s Ark Lab, Huawei Technologies.  
E-mail: [xusongcen@huawei.com](mailto:xusongcen@huawei.com)

sampling operators where downsampling and upsampling are guided by learned indices. The indices are generated dynamically conditioned on the feature map and are learned using a fully convolutional network, termed IndexNet, without extra training supervision. IndexNet is a highly flexible module, which can be used as a plug-in applying to almost all off-the-shelf convolutional networks that have coupled downsampling and upsampling stages. Compared to the fixed max function or bilinear interpolation, learned index functions show potentials for simultaneous boundary and region delineation.

It is worth noting that, IndexNet is a high-level concept and represents a broad family of networks modeling the so-called index function. One can design IndexNet according to the task at hand. In this work, we instantiate and investigate five families of IndexNet. Each family is designed to correspond to different assumptions. Different assumptions result in different capacities of IndexNet and different degrees of floating-point calculations. IndexNet can be incorporated into many CNNs to benefit a number of visual tasks, for instance: i) *image matting*: our MobileNetv2-based [9] model with IndexNet exhibits at least 16.1% improvement against the seminal VGG-16-based DeepMatting baseline [7] on the Composition-1k matting dataset. By further visualizing learned indices, the indices automatically learn to capture the boundaries and textural patterns; ii) *image denoising*: a modified DnCNN model with IndexNet can achieve performance comparable to the baseline DnCNN [10] that has no downsampling stages on the BSD68 and Set12 datasets [11], thus reducing the computational cost and memory consumption significantly; iii) *scene understanding*: consistently improved performance is observed when SegNet [3] is equipped with IndexNet on the SUN RGB-D dataset [12]; and iv) *monocular depth estimation*: IndexNet can also improve the performance of a recent light-weight FastDepth model on the NYUDv2 dataset [13], with almost negligible extra computation cost. Overall, this work has the following main contributions:

- We present an unified perspective of existing upsampling operators with the notion of the index function;
- We introduce Index Networks—a novel family of networks that can be included into standard CNNs to provide dynamic, adaptive downsampling and upsampling capabilities; To the best of our knowledge, IndexNet is the first attempt towards the design of generic upsampling operators;
- We instantiate, investigate five designs of IndexNet and demonstrate their effectiveness on four vision tasks.

The preliminary conference version of this work appeared in [14]. We extend [14] in the following aspects. First, we further propose and investigate two types of light-weight IndexNet. We also compare properties and computational complexity of proposed index networks. Besides image matting in [14], we now apply the proposed methods to many more vision tasks including image denoising, semantic segmentation and monocular depth estimation and report extensive experiment results, not only between index networks but also across different vision tasks.

## 2 LITERATURE REVIEW

Since IndexNet is designed specifically for upsampling stages, we first present a brief review to existing upsampling operators. Considering the dynamic nature of IndexNet, IndexNet also closely relates to another group of networks we call dynamic networks.

### 2.1 Upsampling in Deep Networks

Despite that network architectures have been extensively studied in modern deep CNNs [15], [16], [17], [18], [19], the ways for downsampling and upsampling feature maps are relatively less studied. Since learning a CNN without sacrificing the spatial resolution is computationally expensive and memory intensive, and suffers from limited receptive fields, downsampling operators, such as strided convolution and max/average pooling, are common choices. To recover the resolution, upsampling is thus an essential stage for almost all dense prediction tasks. This poses a fundamental problem about *what is the principal way to recover the resolution of the downsampled feature map (decoding)*. Many upsampling operators therefore have been proposed. The *deconvolution* operator, also known as transposed convolution, was initially used in [1] to visualize convolutional activations and introduced into semantic segmentation [2], but this operator was later found to be harmful to dense prediction due to its default behavior in producing checkerboard artifacts [20]. To avoid this, a follow-up suggestion is the “resize+convolution” paradigm, which has currently become the standard configuration in state-of-the-art semantic segmentation models [5], [6]. Apart from these, *perforate* [21] and *unpooling* [3] are two operators that generate sparse indices to guide upsampling. The indices are able to capture and keep boundary information, but the problem is that two operators can induce too much sparsity after upsampling. Convolutional layers with large filter sizes must follow for densification. In addition, *periodic shuffling* ( $\mathcal{PS}$ ) was introduced in [4] as a fast and memory-efficient upsampling operator for image super-resolution.  $\mathcal{PS}$  recovers resolution by rearranging the feature map of size  $H \times W \times Cr^2$  to  $rH \times rW \times C$ . This operator is also used in some recent segmentation models, e.g., in [22].

Our work is primarily inspired by the unpooling operator [3]. We remark that, it is important to keep the spatial information before the loss of such information occurred in the downsampling of feature maps, and more importantly, to use stored information during upsampling. Unpooling shows a simple and effective case of doing this, but we argue there is much room to improve. In this paper, we illustrate that the unpooling operator is a special form of index function, and we can learn an index function beyond unpooling.

### 2.2 Dynamic Networks

If considering the dynamic property of IndexNet, IndexNet shares a similar spirit with an interesting group of networks—dynamic networks. Dynamic networks are learnable modules that introduce some forms of dynamics into a CNN to extend its modeling capabilities in some aspects. Such dynamics often have clear physical definitions.

Existing dynamic networks also have identical designs: a side-branch localized network that receives the feature map as input, generates dynamics as output and is learned without extra training supervision. We review some widely-cited networks below.

*Spatial Transformer Networks (STNs)* [23]. As the name implies, a STN allows the explicit manipulation of spatial transformation within the network. It achieves this through regressing desired transformation parameters  $\theta$  with a localized network. A spatially-transformed output is then produced by a sampler parameterized by  $\theta$ . This results in a holistic transformation for the feature map. The dynamic property in STNs is reflected by the fact that, given different inputs, the predicted  $\theta$  is different, which adaptively learns some forms of invariance to translation, scale, rotation, etc. The physical meaning of such dynamics corresponds to spatial transformation.

*Dynamic Filter Networks (DFNs)* [24]. A DFN implements a so-called filter generating network to dynamically generate filter parameters on-the-fly. Compared to conventional filter parameters that are initialized, learned, and stayed fixed during inference, filter parameters in DFNs are dynamic and sample-specific. The physical meaning of dynamics in DFNs is obvious—filter kernels. The main difference between DFN and IndexNet lies in the motivation of the design. Dynamic filters are learned for adaptive feature extraction, but learned indices are used for dynamic downsampling and upsampling.

*Deformable Convolutional Networks (DCNs)* [25]. The DCN introduces deformable convolution and deformable RoI pooling. The key idea is to predict offsets for convolutional and pooling kernels. With offsets, convolution and pooling can thus be executed on irregular sampling grids. Since the deformation also depends on the feature map, the DCN is also a dynamic network with a physical meaning of spatial offsets. Unfortunately, these convolutional and pooling operators are still built upon standard max pooling.

*Attention Networks* [26]. Attention networks are a broad family of networks that adopt attention mechanisms. The mechanisms introduce multiplicative interactions between the inferred attention map and the feature map. In computer vision, attention mechanisms are usually referred to spatial attention [27], channel attention [19] or both [28]. These network modules are widely applied in CNNs to force the network focusing on specific regions and therefore to refine feature maps. However, to the best of our knowledge, no attentional module has been designed to deal with the downsampling/upsampling stage.

In contrast to above dynamic networks, IndexNet specializes in upsampling, rather than manipulating filters or refining features. In analogous to these dynamic networks, the dynamics in IndexNet also have a clear physical definition—indices. Such a definition also closely relates to attention networks. Latter in this paper, we show that the downsampling and upsampling operators used with IndexNet can, to some extent, be viewed as attentional operators, which means that indices are attention. For example, max-pooling indices are a form of hard attention.

### 3 AN INDEXING PERSPECTIVE OF UPSAMPLING

With the argument that upsampling operators are index functions, here we offer an unified indexing perspective of upsampling operators. The unpooling operator is straightforward. We can define its index function in a  $k \times k$  local region as an indicator function

$$I_{max}(x) = \mathbb{1}(x = \max(\mathbf{X})), x \in \mathbf{X}, \quad (1)$$

where  $\mathbf{X} \in \mathbb{R}^{k \times k}$ . Similarly, if one extracts indices from the average pooling operator, the index function takes the form

$$I_{avg}(x) = \mathbb{1}(x \in \mathbf{X}). \quad (2)$$

If further using  $I_{avg}(x)$  during upsampling, it is equivalent to the nearest neighbor interpolation. As for the bilinear interpolation and deconvolution operators, their index functions have an identical form

$$I_{bilinear/deconv}(x) = \mathbf{W} \otimes \mathbb{1}(x \in \mathbf{X}), \quad (3)$$

where  $\mathbf{W}$  is the weight/filter of the same size as  $\mathbf{X}$ , and  $\otimes$  denotes the element-wise multiplication. The difference is that,  $\mathbf{W}$  in deconvolution is learned, while  $\mathbf{W}$  in bilinear interpolation depends on coordinates and stays fixed. Indeed, bilinear upsampling has been shown to be a special case of deconvolution [2]. Note that, in this case, the index function generates soft indices. The sense of index for the  $\mathcal{P}\mathcal{S}$  operator [4] is even much clear, because the rearrangement of the feature map per se is an indexing process. Considering  $\mathcal{P}\mathcal{S}$  a tensor  $\mathcal{Z}$  of size  $1 \times 1 \times r^2$  to a matrix  $\mathbf{Z}$  of size  $r \times r$ , the index function can be expressed by the one-hot encoding

$$I_{ps}^l(x) = \mathbb{1}(x = \mathcal{Z}_l), l = 1, \dots, r^2, \quad (4)$$

such that  $\mathbf{Z}_{m,n} = \mathcal{Z}[I_{ps}^l(x)]$ , where  $m = 1, \dots, r$ ,  $n = 1, \dots, r$ , and  $l = (r-1) * m + n$ .  $\mathcal{Z}_l$  denotes the  $l$ -th element of  $\mathcal{Z}$ . A similar notation applies to  $\mathbf{Z}_{m,n}$ .

Since upsampling operators can be unified by the notion of index functions, it is reasonable to think whether one can learn an index function that adaptively captures local spatial patterns.

### 4 LEARNING TO INDEX, TO POOL, AND TO UPSAMPLE

Before introducing concrete designs of IndexNet, we first present a general sense about how learned indices may be used in downsampling and upsampling. We show details in a new index-guided encoder-decoder framework. Our framework is a natural generalization of SegNet, as schematically illustrated in Fig. 2. For ease of exposition, we assume the downsampling and upsampling rates are 2, and the pooling operator has a kernel size of  $2 \times 2$ . The IndexNet module dynamically generates indices given the feature map. The proposed indexed pooling and indexed upsampling operators further receive generated indices to guide the downsampling and upsampling, respectively. In practice, multiple such modules can be combined and used analogous to the max pooling layers for every downsampling and upsampling stage. We provide details as follows.

*IndexNet* models the index as a function of the feature map  $\mathcal{X} \in \mathbb{R}^{H \times W \times C}$ . It generates two index maps for downsampling and upsampling given the input  $\mathcal{X}$ , respectively.

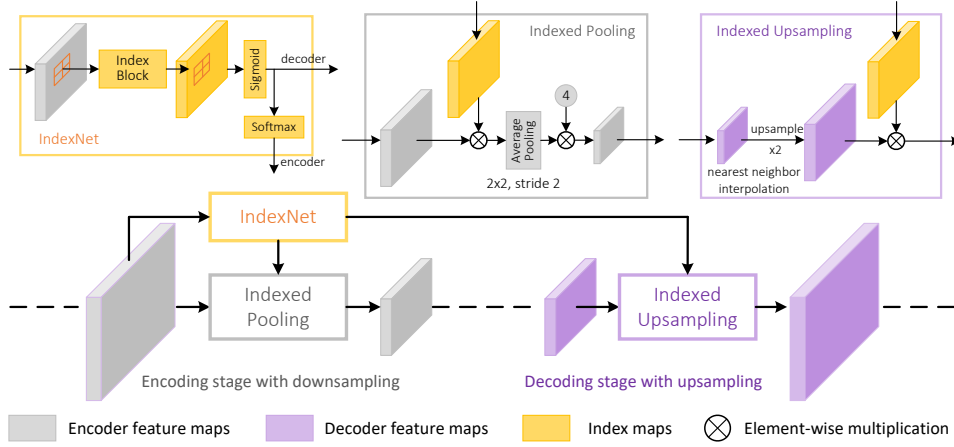


Fig. 2. Index-guided encoder-decoder framework. The proposed IndexNet dynamically predicts indices for individual local regions, conditional on the input local feature map itself. The predicted indices are further used to guide the downsampling in the encoding stage and the upsampling in corresponding decoding stage.

An important concept for the index is that an index can either be represented in a natural order, e.g., 1, 2, 3, ..., or be represented in a logical form, i.e., 0, 1, 0, ..., which means an index map can be used as a mask. In fact, this is how we use the index map in downsampling and upsampling. The predicted index shares the same physical definition of the index in computer science, except that we generate *soft* indices for smooth optimization, i.e., for any index  $i$ ,  $i \in [0, 1]$ .

IndexNet consists of a predefined index block and two index normalization layers. An index block can simply be a heuristically defined function, e.g., a max function, or more generally, a neural network. In this work, the index block is designed to use a fully convolutional network. We will discuss concrete design of index networks in Sections 4.2 and 4.3. Notice that the index maps sent to the encoder and decoder are normalized differently. The decoder index map only goes through a *sigmoid* function such that for any predicted index  $i \in (0, 1)$ . As for the encoder index map, indices of each local region  $L$  are further normalized by a *softmax* function such that  $\sum_{i \in L} i = 1$ . The reason behind the second normalization is to guarantee the magnitude consistency of the feature map after downsampling.

*Indexed Pooling* ( $\mathcal{JP}$ ) executes downsampling using generated indices. Given a local region  $E \in \mathbb{R}^{k \times k}$ ,  $\mathcal{JP}$  calculates a weighted sum of activations and corresponding indices over  $E$  as  $\mathcal{JP}(E) = \sum_{x \in E} I(x)x$ , where  $I(x)$  is the index of  $x$ . It is easy to infer that max pooling and average pooling are special cases of  $\mathcal{JP}$ . In practice, this operator can be easily implemented with an element-wise multiplication between the feature map and the index map, an average pooling layer, and a multiplication of a constant used to compensate the effect of averaging, as instantiated in Fig. 2. The current implementation is equivalent to  $2 \times 2$  2-stride convolution with dynamic kernels, but is more efficient than explicit on-the-fly kernel generation.

*Indexed Upsampling* ( $\mathcal{JU}$ ) is the inverse operator of  $\mathcal{JP}$ .  $\mathcal{JU}$  upsamples  $d \in \mathbb{R}^{1 \times 1}$  that spatially corresponds to  $E$  taking the same indices into account. Let  $I \in \mathbb{R}^{k \times k}$  be the local index map formed by  $I(x)$ s,  $\mathcal{JU}$  upsamples  $d$  as  $\mathcal{JU}(d) = I \otimes d$ , where  $\otimes$  denotes the element-wise multiplication, and  $d$  is of the same size as  $I$  and is upsampled from  $d$

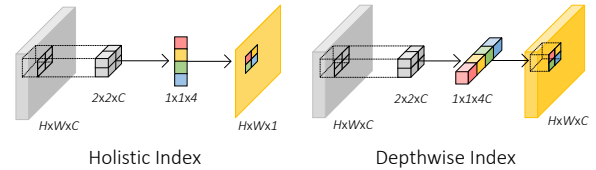


Fig. 3. Conceptual differences between holistic index and depthwise index.

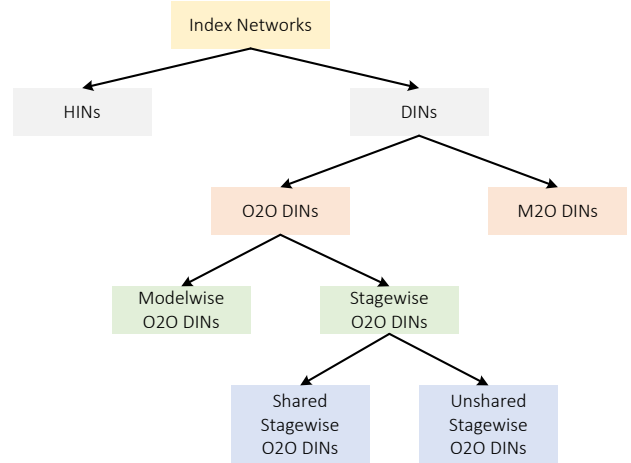


Fig. 4. A taxonomy of proposed index networks.

with the nearest neighbor interpolation.  $\mathcal{JU}$  also relates to deconvolution, but an important difference between  $\mathcal{JU}$  and deconvolution is that, deconvolution applies a fixed kernel to all local regions, even if the kernel is learned, while  $\mathcal{JU}$  upsamples different regions with different kernels (indices).

### 4.1 Index Networks

Here we present a taxonomy of proposed index networks. According to the shape of the output index map, index networks can be first categorized into two branches: *holistic index networks* (HINs) and *depthwise (separable) index networks* (DINs). Their conceptual differences are shown in Fig. 3. HINs learn an index function  $I(\mathcal{X}) : \mathbb{R}^{H \times W \times C} \rightarrow \mathbb{R}^{H \times W \times 1}$ . In this case, all channels of the feature map share a holistic index map. In contrast, DINs learn an index function  $I(\mathcal{X}) : \mathbb{R}^{H \times W \times C} \rightarrow \mathbb{R}^{H \times W \times C}$ , where the index map is of the same size as the feature map.

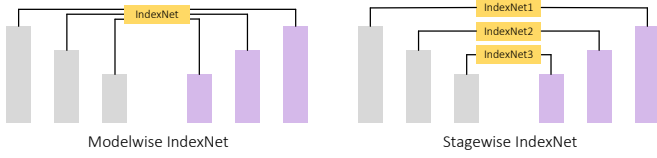


Fig. 5. Modelwise IndexNet vs. stagewise IndexNet.

Since the index map generated by DINs can correspond to individual slices of the feature map, we can incorporate further assumptions into DINs to simplify the designs. If assuming that each slice of the index map only relates to its corresponding slice of the feature map, this gives One-to-One (O2O) assumption and *O2O DINs*. If each slice of the index map relates to all channels of the feature map, this leads to Many-to-One (M2O) assumption and *M2O DINs*. In O2O DINs, one can further consider sharing IndexNet. In the most simplified case, the same IndexNet can be applied to every slice of the feature map and can be shared across different downsampling/upsampling stages, like the max function. We call this IndexNet as *Modelwise O2O DINs*. If an IndexNet is only shared by all feature slices in one stage but is not broadcast to different stages, we call this IndexNet *Shared Stagewise O2O DINs*. Finally, without sharing any parameter in IndexNet (each feature slice has its specific index function), we arrive at the standard design we call *Unshared Stagewise O2O DINs*. Fig. 4 illustrates the tree diagram of these index networks. The difference between modelwise IndexNet and stagewise IndexNet is also shown in Fig. 5. Notice that, HINs and M2O DINs are both stagewise.

As per the above taxonomy of IndexNet, we investigate five families of IndexNet. Each family of IndexNet can be designed to have either linear mappings or nonlinear mappings, as discussed next.

### 4.2 Holistic Index Networks

Recall that HINs learn an index function  $I(\mathcal{X}) : \mathbb{R}^{H \times W \times C} \rightarrow \mathbb{R}^{H \times W \times 1}$ . A naive design choice is to assume a linear relationship between the feature map and the index map.

*Linear HINs.* An example is shown in Fig. 6(a). The network is implemented in a fully convolutional network. It first applies 2-stride  $2 \times 2$  convolution (we assume the downsampling rate is 2) to the feature map of size  $H \times W \times C$ , generating a concatenated index map of size  $H/2 \times W/2 \times 4$ . Each slice of the index map ( $H/2 \times W/2 \times 1$ ) is designed to correspond to the indices of a certain position of all local regions, e.g., the top-left corner of all  $2 \times 2$  regions. The network finally applies a  $\mathcal{PS}$ -like shuffling operator to rearrange the index map to the size of  $H \times W \times 1$ .

In many situations, assuming a linear relationship is not sufficient. An obvious fact is that a linear function even cannot fit the max function. Naturally the second design choice is to include nonlinearity into the network.

*Nonlinear HINs.* Fig. 6(b) illustrates a nonlinear HIN where the feature map is first projected to a map of size  $H/2 \times W/2 \times 2C$ , followed by a batch normalization layer and a ReLU function for nonlinear mappings. We then use point-wise convolution to reduce the channel dimension to an indices-compatible size. The rest transformations follow its linear counterpart.

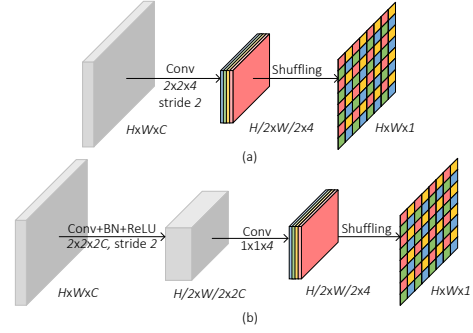


Fig. 6. Holistic index networks. (a) a linear index network; (b) a nonlinear index network.

### 4.3 Depthwise Index Networks

In DINs, we seek  $I(\mathcal{X}) : \mathbb{R}^{H \times W \times C} \rightarrow \mathbb{R}^{H \times W \times C}$ , i.e., each spatial index corresponds to each spatial activation. As aforementioned, this type of networks further has two different high-level design strategies that correspond to two different assumptions.

#### 4.3.1 One-to-One Depthwise Index Networks

O2O assumption assumes that each slice of the index map only relates to its corresponding slice of the feature map. It can be denoted by a local index function  $l(\mathcal{X}) : \mathbb{R}^{k \times k \times 1} \rightarrow \mathbb{R}^{k \times k \times 1}$ , where  $k$  denotes the size of the local region. Since the local index function operates on individual feature slices, we can design whether different feature slices share the same local index function or not. As aforementioned, such a weight sharing strategy could be applied at a model-wise level or at a stagewise level, which gives the following designs of O2O DINs:

- 1) *Modelwise O2O DINs*: the model only has an unique index function that is shared by all feature slices, even in different downsampling and upsampling stages. This is the most light-weight design;
- 2) *Shared Stagewise O2O DINs*: the index function is also shared by feature slices, but every stage has stage-specific IndexNet. This design is also light-weight;
- 3) *Unshared Stagewise O2O DINs*: even in the same stage, different feature slices have distinct local index functions.

Similar to HINs, DINs can also be designed to have linear/nonlinear modeling ability. Fig. 7 shows an example when  $k = 2$ . Note that, in contrast to HINs, DINs follow a multi-column architecture. Each column is responsible for predicting indices specific to a certain spatial location of all local regions. We implement DINs with group convolution.

*Linear O2O DINs.* According to Fig. 7, the feature map first goes through four parallel convolutional layers with the same kernel size. Modelwise O2O DINs and Shared Stagewise O2O DINs only utilize a kernel size of  $2 \times 2 \times 1$ , a stride of 2, and 1 group, while Unshared Stagewise O2O DINs has a kernel size of  $2 \times 2 \times C$ , a stride of 2, and  $C$  groups. One can simply reshape the feature map, i.e., reshaping  $H \times W \times C$  to be  $C \times H \times W \times 1$ , to enable a  $2 \times 2 \times 1$  kernel operating on each  $H \times W \times 1$  feature slice, respectively. All O2O DINs lead to four downsampled feature maps of size  $H/2 \times W/2 \times C$ . The final index map of size  $H \times W \times C$  is composed from the four feature maps

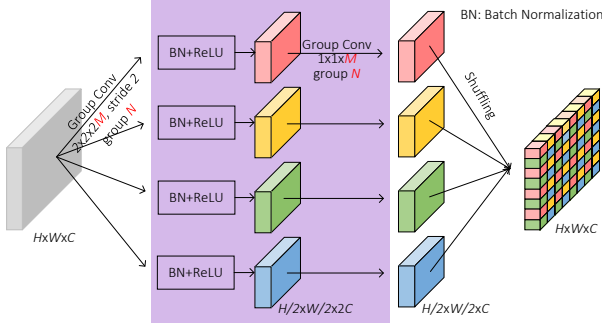


Fig. 7. Depthwise index networks.  $M = 1, N = 1$  for Modelwise O2O DINs and Shared Stagewise O2O DINs;  $M = C, N = C$  for Unshared Stagewise O2O DINs; and  $M = C, N = 1$  for the M2O DINs. The masked modules are invisible to linear networks.

by shuffling and rearrangement. Note that the parameters of four columns are not shared.

*Nonlinear O2O DINs.* Nonlinear DINs can be easily modified from linear DINs by inserting four extra convolutional layers. Each of them is followed by a BN layer and a ReLU unit, as shown in Fig. 7. The rest remains the same as the linear DINs.

### 4.3.2 Many-to-One Depthwise Index Networks

M2O assumption assumes that all feature slices have contributions to each index slice. The local index function is defined as  $l(\mathcal{X}) : \mathbb{R}^{k \times k \times C} \rightarrow \mathbb{R}^{k \times k \times 1}$ . Compared to O2O DINs, the only difference in implementation is the use of standard convolution instead of group convolution, i.e.,  $M = C, N = 1$  in Fig. 7.

## 4.4 Property and Model Complexity

Both HINs and DINs have merits and drawbacks. Here we discuss and highlight some important properties of IndexNet which should be kept in mind when using them in practice. We also present an analysis of computational complexity to HINs and DINs.

**Remark 1.** *Index maps generated by HINs and used by the  $\mathcal{I}\mathcal{P}$  and  $\mathcal{U}$  operators somewhat relate to spatial attention.*

Note that, the holistic index map is shared by all channels of the feature map, which means the index map is required to be expanded to the size of  $H \times W \times C$  when feeding into  $\mathcal{I}\mathcal{P}$  and  $\mathcal{U}$ . Fortunately, many existing packages support implicit expansion over the singleton dimension. This index map could be thought as a collection of local attention maps [26] applied to individual local spatial regions. In this case, the  $\mathcal{I}\mathcal{P}$  and  $\mathcal{U}$  operators can also be referred to “attentional pooling” and “attentional upsampling”. However, it should also be noted that spatial attention has no pooling or upsampling behavior like  $\mathcal{I}\mathcal{P}$  and  $\mathcal{U}$ .

**Remark 2.** *HINs are more flexible than DINs and much more friendly for decoder design.*

Since the index map generated by HINs is shared by all channels of the feature map, the decoder feature map can reserve its expressibility without forcibly reducing its dimensionality to fit the shape of the index map during upsampling. This gives much flexibility for decoder design, while it is not the case for DINs.

TABLE 1  
A Comparison of Model Complexity of Different Index Networks

IndexNet	Type	# Param.
HINs	L	$K \times K \times C \times 4$
	NL	$K \times K \times C \times 2C + 2C \times 4$
	NL+C	$2K \times 2K \times C \times 2C + 2C \times 4$
Modelwise O2O DINs	L	$(K \times K) \times 4$
	NL	$(K \times K \times 2 + 2) \times 4$
	NL+C	$(2K \times 2K \times 2 + 2) \times 4$
Shared Stagewise O2O DINs	L	$(K \times K) \times 4$
	NL	$(K \times K \times 2 + 2) \times 4$
	NL+C	$(2K \times 2K \times 2 + 2) \times 4$
Unshared Stagewise O2O DINs	L	$(K \times K \times C) \times 4$
	NL	$(K \times K \times 2C + 2C \times C) \times 4$
	NL+C	$(2K \times 2K \times 2C + 2C \times C) \times 4$
M2O DINs	L	$(K \times K \times C \times C) \times 4$
	NL	$(K \times K \times C \times 2C + 2C \times C) \times 4$
	NL+C	$(2K \times 2K \times C \times 2C + 2C \times C) \times 4$

L: Linear; NL: Nonlinear; C: Context

**Remark 3.** *The number of parameters in Modelwise O2O DINs and Shared Stagewise O2O DINs is independent of the dimensionality of feature maps.*

Modelwise O2O DINs and Shared Stagewise O2O DINs both have shared IndexNet(s). No matter how large the model capacity is or how wide the feature channels are, the number of parameters in Modelwise O2O DINs remains at a constant level, and that in Shared Stagewise O2O DINs is only proportional to the number of downsampling/upsampling stages. This is a desired property for those who want the dynamic behavior of IndexNet without increasing the model capacity obviously. However, these two types of IndexNet may be limited to capture sophisticated local patterns.

**Remark 4.** *M2O DINs have the most powerful modeling capability among other IndexNets, but also introduce many extra parameters and memory consumption.*

M2O DINs have higher capacity than HINs and O2O DINs due to the use of standard convolution. M2O DINs can capture much versatile local patterns but also are at a risk of overfitting. They should be used with care.

**Remark 5.** *IndexNet can learn with weak context.*

Another desirable property of IndexNet is that they can predict the indices even from a large local feature map, e.g.,  $l(\mathcal{X}) : \mathbb{R}^{2k \times 2k \times C} \rightarrow \mathbb{R}^{k \times k \times 1}$ . This allows IndexNet to learn with *weak context*. An intuition behind this idea is that, if one identifies a local maximum point from a  $k \times k$  region, its surrounding  $2k \times 2k$  region can further support whether this point is a part of a boundary or just an isolated noise point. This idea can be easily implemented by enlarging the convolutional kernel size and with appropriate padding.

In Table 1, we summarize the model complexity of different index networks used at a single downsampling and upsampling stage. We assume the convolution kernel has a size of  $K \times K$  applied on a  $C$ -channel feature map. The number of parameters in BN layers is excluded. When considering weak context, we assume the kernel size is  $2K \times 2K$ . Since  $C \gg K$ , generally we have the model complexity  $M2O \text{ DINs} > HINs > Unshared \text{ Stagewise O2O DINs} > Shared \text{ Stagewise O2O DINs} > Modelwise \text{ O2O DINs}$ .

## 5 APPLICATIONS

In this section, we show several applications of IndexNet on the tasks of image matting, image denoising, scene understanding, as well as monocular depth estimation. Since IndexNet introduces extra parameters and calculations, in most evaluations we also showcase the increased number of parameters and the amount of floating-point calculations.

### 5.1 Image Matting

We first evaluate IndexNet on the task of image matting. Image matting is defined as a problem of estimating soft foreground from images. This problem is ill-posed due to the fact that solving a linear system of 7 unknown variables with only 3 known inputs: given the RGB color at pixel  $i$ ,  $I_i$ , one needs to estimate the corresponding foreground color  $F_i$ , background color  $B_i$ , and matte  $\alpha_i$ , such that  $I_i = \alpha_i F_i + (1 - \alpha_i) B_i$ , for any  $\alpha_i \in [0, 1]$ . Previous methods have extensively studied this problem from a low-level view [29], [30], [31], [32]; and particularly, they have been designed to solve the above matting equation. Despite being theoretically elegant, these methods heavily rely on the color cues, rendering failures of matting in general natural scenes where colors are not reliable. With the tremendous success of deep CNNs in high-level vision tasks [2], [15], [33], deep matting methods are emerging. Some initial attempts appeared in [34] and [35], where classic matting approaches, such as closed-form matting [32] and KNN matting [29], are still used as the backends in deep networks. Although the networks are trained end-to-end and can extract powerful features, the final performance is limited by the conventional backends. These attempts may be thought as semi-deep matting. Recently fully-deep image matting was proposed [7]. In [7] the authors presented the first deep image matting approach (DeepMatting) based on SegNet [3] and significantly outperformed other competitors. In this application, we treat DeepMatting as our baseline.

It is worth noting that image matting is particularly suitable for evaluating the effectiveness of IndexNet, because the quality of learned indices can be visually observed from inferred alpha mattes. We mainly conduct experiments on the Adobe Image Matting dataset [7]. This is so far the largest publicly available matting dataset. The training set has 431 foreground objects and ground-truth alpha mattes.<sup>1</sup> Each foreground is composited with 100 background images randomly chosen from MS COCO [36]. The validation set termed Composition-1k includes 100 unique objects. Each of them is composited with 10 background images chosen from Pascal VOC [37]. Overall, we have 43100 training images and 1000 testing images. We evaluate the results using widely-used Sum of Absolute Differences (SAD), Mean Squared Error (MSE), and perceptually-motivated Gradient (Grad) and Connectivity (Conn) errors [38]. The evaluation code implemented by [7] is used. In what follows, we first describe our modified MobileNetv2-based architecture and training details. We then perform extensive ablation studies

1. The original paper said there were 491 images, but the released dataset only included 431 images. Among missing images, 38 of them were said double counted, and the other 24 of them were not released due to the copyright issue. As a result, we at least has 4.87% training data less than the original paper.

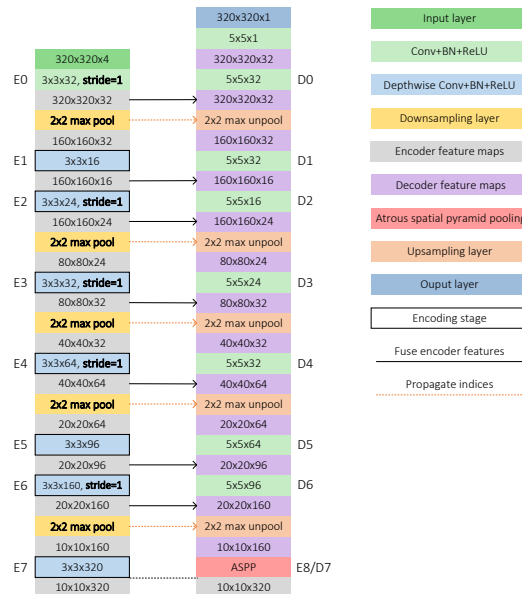


Fig. 8. Customized MobileNetv2-based encoder-decoder network architecture. Our modifications are boldfaced.

to justify choices of model design, make comparisons of different index networks, and visualize learned indices.

#### 5.1.1 Network Architecture and Implementation Details

Our implementation is based on PyTorch [39]. Here we describe the network architecture used and some essential training details.

*Network Architecture.* We build our model based on MobileNetv2 [9] with only slight modifications to the backbone. An important reason why we choose MobileNetv2 is that this lightweight model allows us to infer high-resolution images on a single GPU (the inference can be performed on the GTX 1070 processing up to  $1920 \times 1080$  high-resolution images), while other high-capacity backbones cannot. The basic network configuration is shown in Fig. 8. It also follows the encoder-decoder paradigm same as SegNet. We simply change all 2-stride convolution to be 1-stride and attach 2-stride  $2 \times 2$  max pooling after each encoding stage for downsampling, which allows us to extract indices. If applying the IndexNet idea, max pooling and unpooling layers can be replaced with  $\mathcal{P}$  and  $\mathcal{U}$ , respectively. We also investigate alternative ways for low-level feature fusion and whether encoding context (Section 5.1.2). Notice that, the matting refinement stage [7] is not considered in this paper.

*Training Details.* To enable a direct comparison with deep matting [7], we follow the same training configurations used in [7]. The 4-channel input concatenates the RGB image and its trimap. We follow exactly the same data augmentation strategies, including  $320 \times 320$  random cropping, random flipping, random scaling, and random trimap dilation. All training samples are created on-the-fly. We use a combination of the alpha prediction loss and the composition loss during training as in [7]. Only losses from the unknown region of the trimap are calculated. Encoder parameters are pretrained on ImageNet [40]. The parameters of the 4-th input channel are initialized with zeros. All other parameters are initialized with the improved Xavier [41]. The Adam optimizer [42] is used. We update parameters with

TABLE 2  
Ablation Study of Design Choices

No.	Architecture	Backbone	Fusion	Indices	Context	OS	SAD	MSE	Grad	Conn
B1	DeepLabv3+ [6]	MobileNetv2	Concat	No	ASPP	16	60.0	0.020	39.9	61.3
B2	RefineNet [5]	MobileNetv2	Skip	No	CRP	32	60.2	0.020	41.6	61.4
B3	SegNet [7]	VGG16	No	Yes	No	32	<b>54.6</b>	<b>0.017</b>	36.7	55.3
B4	SegNet	VGG16	No	No	No	32	122.4	0.100	161.2	130.1
B5	SegNet	MobileNetv2	No	Yes	No	32	60.7	0.021	40.0	61.9
B6	SegNet	MobileNetv2	No	No	No	32	78.6	0.031	101.6	82.5
B7	SegNet	MobileNetv2	No	Yes	ASPP	32	58.0	0.021	39.0	59.5
B8	SegNet	MobileNetv2	Skip	Yes	No	32	57.1	0.019	36.7	57.0
B9	SegNet	MobileNetv2	Skip	Yes	ASPP	32	56.0	<b>0.017</b>	38.9	55.9
B10	UNet	MobileNetv2	Concat	Yes	No	32	54.7	<b>0.017</b>	34.3	<b>54.7</b>
B11	UNet	MobileNetv2	Concat	Yes	ASPP	32	54.9	<b>0.017</b>	<b>33.8</b>	55.2

Fusion: fuse encoder features; Indices: max-pooling indices (when Indices is ‘No’, bilinear interpolation is used for upsampling); CRP: chained residual pooling [5]; ASPP: atrous spatial pyramid pooling [6]; OS: output stride. The lowest errors are boldfaced.

30 epochs (around 90,000 iterations). The learning rate is initially set to 0.01 and reduced by  $10\times$  at the 20-th and 26-th epoch respectively. We use a batch size of 16 and fix the BN layers of the backbone.

### 5.1.2 Results on the Adobe Image Matting Dataset

*Ablation Study on Model Design.* To establish a better baseline comparable to DeepMatting, here we first investigate strategies for fusing low-level features (no fusion, skip fusion as in ResNet [17] or concatenation as in UNet [43]) and whether encoding context for image matting. 11 baselines are consequently built to justify model design. Results on the Composition-1k testing set are reported in Table 2. B3 is cited from [7]. We can make the following observations:

- i) Indices are of great importance. Matting can significantly benefit from only indices (B3 vs. B4, B5 vs. B6);
- ii) State-of-the-art semantic segmentation models cannot be directly applied to image matting (B1/B2 vs. B3);
- iii) Fusing low-level features help, and concatenation works better than the skip connection but at a cost of increased computation (B6 vs. B8 vs. B10 or B7 vs. B9 vs. B11);
- iv) Our intuition tells that the context may not help a low-level task like matting, while results show that encoding context is generally encouraged (B6 vs. B7 or B8 vs. B9 or B10 vs. B11). Indeed, we observe that the context sometimes can help to improve the quality of the background;
- v) A MobileNetv2-based model can work as well as a VGG-16-based one with appropriate design choices (B3 vs. B11).

For the following experiments, we now mainly use B11.

*Ablation Study on Index Networks.* Here we compare different index networks and justify their effectiveness. The configurations of index networks used in the experiments follow Figs. 6 and 7. We primarily investigate the  $2\times 2$  kernel with a stride of 2. Whenever the weak context is considered, we use a  $4\times 4$  kernel in the first convolutional layer of index networks. To highlight the effectiveness of HINs, we further build a baseline called *holistic max index* (HMI) where max-pooling indices are extracted from a squeezed feature map  $\mathcal{X}' \in \mathbb{R}^{H\times W\times 1}$ .  $\mathcal{X}'$  is generated by applying the max function along the channel dimension of  $\mathcal{X} \in \mathbb{R}^{H\times W\times C}$ . Furthermore, since IndexNet increases extra parameters, we introduce another baseline *B11-1.4* where the width multiplier of MobileNetV2 is adjusted to be 1.4 to increase

the model capacity. Results on the Composition-1k testing dataset are listed in Table 3. We observe that, most index networks reduce the errors notably, except for some low-capacity IndexNet modules (due to limited modeling capabilities). In particular, nonlinearity and the context generally have a positive effect on deep image matting, but they do not work effectively in O2O DINs. A possible reason may be that the limited dimensionality of the intermediate feature map is not sufficient to model complex patterns in matting. Compared to holistic max index, the direct baseline of HINs, the best HIN (“Nonlinear+Context”) has at least 12.3% relative improvement. Compared to B11, the baseline of DINs, M2O DIN with “Nonlinear+Context” exhibits at least 16.5% relative improvement. Notice that, our best model outperforms the DeepMatting approach [7] that even has the refinement stage. In addition, according to the results of B11-1.4, the performance improvement does not come from increased parameters. Some qualitative results are shown in Fig. 9. Our predicted mattes show improved delineation for edges and textures like hair and water drops.

*Ablation Study on Index Normalization.* Index normalization actually has an important effect on the final performance. Here we justify this by evaluating different normalization choices to the index maps. Aside from the sigmoid function used for the decoder and the sigmoid+softmax function for the encoder, we compare other three different combinations of normalization choices, as listed in Table 4. The experiment is conducted based on M2O DIN with the setting of ‘Nonlinear’+‘Context’. According to the results, it is clear that keeping the magnitude consistency during downsampling matters. In fact, both max pooling and average pooling satisfy this property naturally, and the normalization design is inspired from this fact.

*Index Map Visualization.* It is interesting to see what indices are learned by IndexNet. For the holistic index, the index map itself is a 2D matrix and is easily to be visualized. Regarding the depthwise index, we squeeze the index map along the channel dimension and calculate the average responses. Two examples of learned index maps are visualized in Fig. 10. We observe that, initial random indices have poor delineation for edges, while learned indices automatically capture the complex structural and textual patterns, e.g., the fur of the dog, and even air bubbles in the water.



model, it can effectively compensate the loss of spatial information, achieving performance comparable to or even better than the network without downsampling. In this way, despite the number of parameters increases, both floating-point calculations and memory consumption have a notable reduction. We choose DnCNN [10] as our baseline and justify this point on standard benchmarks. We follow the experimental setting of [49] that uses a 400-image training set. The performance is reported on a 68-image Berkeley segmentation dataset (BSD68) and the other 12-image test set (Set12). The networks are trained for Gaussian denoising, with three noise levels, i.e.,  $\sigma = 15, 25$  and  $50$ . Peak Signal-to-Noise Ratio (PSNR) and Structural SIMilarity index (SSIM) are used as evaluation metrics.

### 5.2.1 Network Architecture and Implementation Details

*Network Architecture.* We use the 17-layer DnCNN model [10], implemented by PyTorch. To enable the use of IndexNet, we modify DnCNN to a SegNet-like architecture with 3 downsampling and upsampling stages (the input image size is  $40 \times 40$ ). The number of layers remains the same to ensure a relatively fair comparison. Fig. 11 illustrates the original DnCNN and our modified architecture. The first 9 layers follow VGG-16 except the first layer is a single-channel input, and the rest are 7 decoding layers formed by unpooling and convolution and the final prediction layer. All convolutional operations utilize  $3 \times 3$  kernels. To incorporate IndexNet, it is straightforward to replace max pooling and unpooling with  $\mathcal{P}$  and  $\mathcal{U}$ .

*Training Details.* We follow the same experimental configurations used in [10]. At each epoch,  $40 \times 40$  image patches are cropped from multiple scales (0.7, 0.8, 0.9, 1) with a stride of 10 and are added with Gaussian noise of a certain noise level ( $\sigma = 15, 25$ , or  $50$ ); image patches are further augmented with random flipping and random rotation. This results in around 240,000 training samples.  $\ell_2$  loss is used. All networks are trained from scratch with a batch size of 128. Model parameters are initialized with the improved Xavier [41]. The Adam optimizer is also used. Parameters are updated with 60 epochs. The learning rate is initially set to 0.001 and reduced by  $10\times$  at the 45-th and 55-th epoch, respectively.

### 5.2.2 Results on the BSD68 and Set12 Datasets

Besides the DnCNN baseline, we also report the performance of our modified DnCNN-SegNet with max pooling and unpooling. Results are shown in Table 5. It can be observed that, simply downsampling with max pooling and upsampling by unpooling as in DnCNN-SegNet lead to significant drops in both PSNR (generally  $> 1dB$ ) and SSIM ( $> 0.1$ ). This suggests spatial information plays an important role in image denoising. A reason may be that the denoising process is content-irrelevant (the model is unaware of regions coming from the foreground or the background). Downsampling without recording sufficient spatial information (only the boundary information is not sufficient) impedes the model from recovering the appearance and the structure in the original image. Interestingly, after IndexNet is inserted into downsampled DnCNN, the loss of PSNR and SSIM is effectively compensated. The compensation behaviors can be observed from almost all types

of IndexNet, except the two cases in Modelwise O2O DINs with nonlinearity. The poor performance of Modelwise O2O DINs may attribute to insufficient modeling ability. It is particularly obvious when  $\sigma = 50$ . If we remove Modelwise O2O DINs, we find that, nonlinearity and weak context generally have a positive effect on image denoising, and the effectiveness of different IndexNets is similar. Hence, Shared Stagewise O2O DINs appear to be a preferred choice due to slightly increased parameters and negligible extra computation cost.

## 5.3 Semantic Segmentation

Here we choose the task of semantic segmentation to evaluate IndexNet. Semantic segmentation models aim at predicting a dense labeling map for each image where each pixel is labeled into one category. Fully convolutional networks [2] (FCNs) are the first successful attempt to apply CNNs to semantic segmentation. Since the proposition of [2], FCN-based encoder-decoder architectures have been studied extensively [3], [5], [6], [50], [51]. Since the relative positions between different categories affect semantic segmentation significantly, a majority of efforts have been made to model rich contextual information into the network, in both parametric and non-parametric way. Although SegNet [3] is not the state-of-the-art model, we choose it as our baseline because IndexNet is primarily inspired by the unpooling operator in SegNet. The clean design and symmetric encoder-decoder structure of SegNet also make it suitable for inserting IndexNet to highlight its effectiveness. We follow the experimental setting in [3] and report performance on the SUN RGB-D [12] dataset. The SUN RGB-D dataset has 5285 training images and 5050 testing images. It includes 37 categories. This dataset is challenging due to a large amount of small objects presented. Only three RGB channels are used as our network input. The standard mean Intersection-over-Union (mIoU) is used as the evaluation metric.

### 5.3.1 Network Architecture and Implementation Details

*Network Architecture.* The architecture of SegNet is simple. It employs the first 13 layers of the VGG-16 model pretrained on ImageNet as the encoder. The decoder utilizes unpooling for upsampling. Each unpooling layer is followed by the same number of convolutional layers as in the corresponding encoder stage. Overall, SegNet has 5 downsampling and 5 upsampling stages. Convolutional layers in the decoding stage mainly play a role to smooth the feature maps generated by unpooling. To insert IndexNet, the only modification is to replace max pooling and unpooling layers with  $\mathcal{P}$  and  $\mathcal{U}$ , respectively, which is straightforward.

*Training Details.* The VGG-16 model pretrained on ImageNet with BN layers is used. We employ the standard data augmentation strategies: random scaling, random cropping  $320 \times 320$  sub-images, and random horizontal flipping. We learn the model with the standard softmax loss. Encoder parameters are pretrained on ImageNet. All other parameters are initialized with the improved Xavier [41]. The SGD optimizer [42] is used with a momentum of 0.9 and a weight decay of 0.0001. We train the model with a batch size of 16 for 300 epochs (around 90,000 iterations). The learning rate is initially set to 0.01 and reduced by  $10\times$  at the 250-th and

TABLE 5  
Average PSNR (dB) and SSIM Results of Various Noise Levels on the BSD68 and Set12 Image Denoising Benchmarks

Method		#Param.	GFLOPs	BSD68			Set12		
Noise Level				15	25	50	15	25	50
DnCNN [10]		0.56M	25.89	31.74/0.9410	29.22/0.9015	26.23/0.8269	32.87/0.9544	30.42/0.9296	27.17/0.8775
DnCNN-SegNet		7.09M	18.14	30.74/0.9278	28.27/0.8752	24.88/0.7437	31.91/0.9395	28.98/0.8881	24.99/0.7485
NL	C	Δ							
				HINs					
		+7.17K	18.16	31.13/0.9357	29.02/0.8997	26.29/0.8281	32.71/0.9536	30.28/0.9285	27.20/0.8789
✓		+0.69M	19.30	31.15/0.9356	29.01/0.8999	26.29/0.8301	32.77/0.9537	30.36/0.9295	27.18/0.8799
✓	✓	+2.76M	22.75	31.20/0.9365	29.05/0.9004	26.30/0.8305	32.79/0.9541	30.37/0.9300	27.22/0.8804
				Modelwise O2O DINs					
		+16	18.14	31.22/0.9366	29.06/0.9002	25.84/0.8294	32.83/0.9545	30.42/0.9302	26.21/0.8782
✓		+56	18.14	30.64/0.9255	27.39/0.8391	26.15/0.6776	31.92/0.9386	27.97/0.8330	24.14/0.6747
✓	✓	+152	18.14	30.87/0.9296	27.70/0.8617	24.09/0.6939	32.23/0.9432	28.31/0.8677	23.85/0.6634
				Shared Stagewise O2O DINs					
		+48	18.14	31.14/0.9364	29.05/0.9002	26.32/0.8310	32.80/0.9542	30.41/0.9302	27.24/0.8807
✓		+168	18.14	31.20/0.9365	28.97/0.9000	26.33/0.8272	32.83/0.9545	30.43/0.9302	27.24/0.8801
✓	✓	+456	18.14	31.22/0.9366	29.07/0.9004	26.31/0.8311	32.82/0.9543	30.41/0.9300	27.27/0.8814
				Unshared Stagewise O2O DINs					
		+7.17K	18.16	31.17/0.9366	28.25/0.8944	25.02/0.8235	32.80/0.9544	30.23/0.9286	26.41/0.8675
✓		+25.1K	18.19	31.25/0.9368	29.06/0.9002	26.33/0.8306	32.77/0.9541	30.43/0.9303	27.29/0.8804
✓	✓	+68.1K	18.32	31.21/0.9364	27.68/0.8740	26.33/0.8312	32.83/0.9544	30.32/0.9288	27.24/0.8807
				M2O DINs					
		+1.38M	20.44	31.22/0.9365	29.03/0.9005	26.33/0.8316	32.82/0.9544	30.42/0.9302	27.28/0.8812
✓		+3.45M	23.88	31.23/0.9368	29.07/0.9002	26.26/0.8278	32.84/0.9546	30.44/0.9304	27.28/0.8808
✓	✓	+11.7M	37.67	31.23/0.9365	29.06/0.8996	26.34/0.8315	32.82/0.9545	30.43/0.9301	27.29/0.8803

NL: Non-Linearity; C: Context. Δ indicates increased parameters compared to the SegNet-DnCNN baseline. GFLOPs are measured on a  $224 \times 224 \times 1$  input.

280-th epoch, respectively. The BN layers of the encoder are fixed.

### 5.3.2 Results on the SUN RGB-D Dataset

As per the experimental results shown in Table 6, all index networks bring improvements over the baseline, among which Modelwise and Shared Stagewise O2O DINs improve the baseline with few extra parameters and GFLOPs. Compared with other types of IndexNet, M2O DINs and HINs (particularly under the setting of ‘Nonlinear’+‘Context’) increase many parameters and GFLOPs, but do not exhibit obvious superiority. These two types of IndexNet may be excluded from candidates for semantic segmentation. Another interesting observation is that, ‘Weak Context’ does not help in this task. A possible reason is that semantic segmentation needs the much large-scale context, e.g., background and category-level cues [52]. From the qualitative results shown in Fig. 12, we can see that the improvement comes from the ability of IndexNet suppressing fractured predictions that frequently appears in the baseline SegNet. This illustration also confirms the superiority of IndexNet for simultaneous region and boundary predictions (SegNet has good predictions on boundaries but poor performance on regions).

## 5.4 Monocular Depth Estimation

Finally, we demonstrate the effectiveness of IndexNet on the task of monocular depth estimation. Estimating per-pixel depth from a single image benefits many visual tasks yet is still an open and ill-posed problem, because one needs to recover 3D information from a 2D RGB image. This problem is conventionally addressed using binocular vision with images taken from different views. With deep learning, significant progress has been witnessed in this field [53], [54], [55], [56], [57]. In this application, we choose a recently proposed FastDepth [57] as our baseline due to its



Fig. 12. Scene understanding results on the SUNRGB-D dataset. From left to right, the original image, ground-truth, SegNet, and ours (Shared Stagewise O2O DIN with ‘Nonlinear’).

clean structure, which is important to highlight the role of IndexNet. We compare the performance of the architectures with/without IndexNet on the NYUv2 dataset [13] with the official train/test split. To be in consistent with [57], the following measures are used to quantify the performance:

- root mean squared error (rmse):  $\sqrt{\frac{1}{T} \sum_{i=1}^T (d_i - g_i)^2}$
- thresholded accuracy: percentage (%) of  $d_1$ , s.t.  $\max\left(\frac{d_1}{g_1}, \frac{g_1}{d_1}\right) = \delta_1 < 1.25$ .

### 5.4.1 Network Architecture and Implementation Details

*Network Architecture.* FastDepth is a clean encoder-decoder architecture, with MobileNet as its backbone. The authors evaluated several upsampling strategies during decoding. Here we choose the NNConv5 upsampling strategy used in [57], where upsampling is implemented by  $\times 2$  nearest neighbor interpolation and  $5 \times 5$  convolution. This is the best upsampling option evaluated by the authors. Hence, our entire baseline is FastDepth-NNConv5: downsampling with 2-stride convolution and upsampling through nearest neighbor interpolation. We also add another baseline by changing

TABLE 6  
Performance on the SUN RGB-D Dataset

Method		#Param.	GFLOPs	mIoU
SegNet [3]		24.96M	24.76	32.47
NL	C	$\Delta$		
HINs				
		+23.55K	24.79	33.25
✓		+4.90M	26.40	33.11
✓	✓	+19.55M	31.28	33.31
Modelwise O2O DINs				
		16	24.76	33.18
✓		56	24.76	33.70
✓	✓	152	24.77	33.26
Shared Stagewise O2O DINs				
		80	24.76	33.26
✓		280	24.76	<b>33.97</b>
✓	✓	760	24.77	33.41
Unshared Stagewise O2O DINs				
		0.02M	24.79	33.27
✓		0.08M	24.82	33.59
✓	✓	0.22M	24.96	33.50
M2O DINs				
		+9.76M	28.02	33.28
✓		+24.44M	32.90	33.51
✓	✓	+83.02M	52.42	33.48

NL: Non-Linearity; C: Context.  $\Delta$  indicates increased parameters compared to the SegNet baseline. GFLOPs are measured on a  $224 \times 224 \times 3$  input. The best performance is boldfaced.

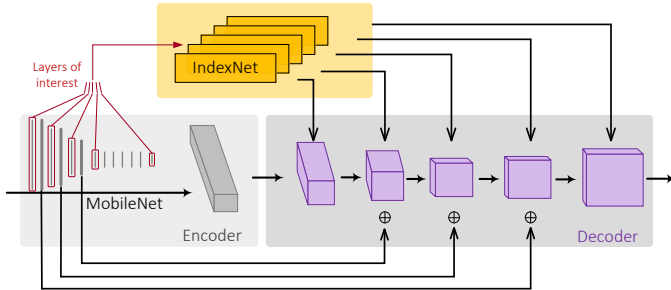


Fig. 13. Our modified FastDepth [57] architecture.

the 2-stride convolution in FastDepth-NNConv5 to be 1-stride followed by max-pooling, named as FastDepth-P-NNConv5. This setting is closer compared to that used in IndexNet. IndexNet can be easily inserted into FastDepth. Our modified architecture is shown in Fig. 13. Similar to the modifications used in the matting network, 2-stride convolution layers in the encoder are changed to be 1-stride, followed by  $\mathcal{J}\mathcal{P}$ . The nearest neighbor upsampling in the decoder is also replaced with  $\mathcal{J}\mathcal{U}$ .

*Training Details.* We follow similar training settings used by FastDepth [57].  $\ell_1$  loss is used. Random rotation, random scaling and random horizontal flipping are used for data augmentation. The initial learning rate is set to 0.01 and reduced by  $\times 10$  every 5 epochs. SGD optimizer is used with a momentum of 0.9 and a weight decay of 0.0001. Encoder weights are pretrained on ImageNet [40]. A batch size of 16 is used to train the network for 30 epochs in total.

### 5.4.2 Results on the NYUDv2 Dataset

Quantitative results are reported in Table 7. We observe that nearly all types of IndexNet improve the performance compared to the baselines except for the most lightweight design—linear Modelwise O2O DIN. A explanation perhaps is that only 16 parameters are not sufficient to model local variations of high-dimensional feature maps.



Fig. 14. Qualitative results on the NYUDv2 dataset. From left to right, the original image, ground-truth, FastDepth-NNConv5, and ours (Unshared Stagewise O2O DIN with ‘Linear’).

TABLE 7  
RMSE and Delta1 results on the NYUDv2 dataset.

Method		#Param.	GFLOPs	RMSE	Delta1
FastDepth-NNConv5		3.96M	0.69	0.567	0.781
FastDepth-P-NNConv5		3.96M	1.01	0.577	0.778
NL	C	$\Delta$			
HINs					
		+31.23K	1.03	0.566	0.784
✓		+11.17M	2.65	0.565	0.786
✓	✓	+44.62M	7.53	0.559	0.787
Modelwise O2O DINs					
		+16	1.02	0.569	0.778
✓		+56	1.02	0.568	0.785
✓	✓	+152	1.02	0.564	0.786
Shared Stagewise O2O DINs					
		+80	1.02	0.562	0.783
✓		+280	1.02	0.565	0.786
✓	✓	+760	1.02	0.567	0.783
Unshared Stagewise O2O DINs					
		+31.23K	1.03	<b>0.556</b>	<b>0.789</b>
✓		+0.11M	1.06	0.564	0.786
✓	✓	+0.30M	1.16	0.562	0.788
M2O DINs					
		+22.30M	4.27	0.563	0.783
✓		+55.78M	9.15	0.562	0.786
✓	✓	+189.57M	28.67	0.565	0.787

NL: Non-Linearity; C: Context.  $\Delta$  indicates increased parameters compared to the FastDepth baseline. GFLOPs are measured on a  $224 \times 224 \times 3$  input. The best performance is boldfaced.

In addition, the effect of nonlinearity and weak context is marginal, which may be neglected for depth prediction. It is worth noting that, Unshared Stagewise O2O DINs (with only linear mappings) bring obvious improvements with only reasonably increased parameters. This may be the recommended setting for depth estimation. HINs and M2O DINs increase a large amount of parameters and floating-point calculations because of the high dimensionality of feature maps, while the improved performance is not proportional to such a high cost. When feature maps are high-dimensional, these two types of IndexNet should be avoided. Some qualitative results are further illustrated in Fig. 14. It is clear that IndexNet has better boundary delineation than the baseline, e.g., the edge of the desk, and the contour of the woman.

### 5.5 Suggestions Towards Good Practices

As a summary of our evaluations, here we provide some guidelines for anyone who wants to try the idea of IndexNet:

- 1) Although IndexNet appears to be effective in different tasks, there is no general rule to choose an optimal setting (e.g., linear or nonlinear) or even a desired type of IndexNet (HINs or DINs) given a certain visual task. However, there does exist some patterns to follow. In image matting, the best IndexNet configuration is “M2O DINs+Nonlinearity+Context”. This configuration is also true for image denoising, where M2O DINs have the most stable behavior, especially when  $\sigma = 50$ . The capacity of IndexNet may have something to do with the complexity of local patterns. M2O DINs may be taken into account if a visual task is detail- or boundary-sensitive, but one should also be aware of the increased model parameters and computation costs, especially when the feature maps are high-dimensional;
- 2) If one prefers the flexibility of decoder design, e.g., squeezing/enlarging the dimensionality of the decoder feature map, HINs are good choices, because DINs only generate index maps whose dimensionality is identical to the input feature map;
- 3) If one has to trade off between the model complexity and computation cost, particularly in light-weight models or in real-time applications, Shared Stagewise O2O DINs are the first-class choices. Model parameters increased by Shared Stagewise O2O DINs are identical to Modelwise O2O DINs, and the extra GFLOPs are also negelectable. However, Shared Stagewise O2O DINs generally work better than Modelwise O2O DINs in all applications, which implies one should devise an index function for each stage respectively;
- 4) It is worth noting that, the implementation of IndexNet in its current form has some limitations. Our current implementation mainly performs single-point upsampling—each upsampled feature point is only associated with a single point. In this sense, we may not simulate the behavior of bilinear interpolation where each upsampled point is determined by multiple points of a local region. If one wants to simulate bilinear interpolation, the first step of  $\mathcal{JP}$  should be replaced by zeros stuffing instead of nearest neighbor interpolation, and the size of learned indices should be odd, e.g.,  $3 \times 3$  for an upsampling factor of 2. Further investigations are out of the scope of this work.

## 6 CONCLUSION

Inspired by an observation in image matting, we have delved deep into the role of indices and presented an unified perspective of upsampling operators using the notion of index function. We showed that an index function can be learned within a proposed index-guided encoder-decoder framework. In this framework, indices are learned with a flexible network module termed IndexNet, and are used to guide downsampling and upsampling using two operators called  $\mathcal{JP}$  and  $\mathcal{JU}$ . IndexNet itself is also a sub-framework that can be designed depending on the task at hand. We instantiated, investigated five index networks, compared their conceptual differences, discussed their properties, and demonstrated their effectiveness on two low-level visual tasks and two high-level tasks. While there may appear an optimal type of IndexNet given a specific task, in most cases

the improved performance is a matter of whether IndexNet is used or not. Overall, we believe that IndexNet is an important step towards generic upsampling operators for deep networks.

Our model is simple with much room for improvement. It would be interesting to design other types of IndexNet and to see applications of IndexNet to other dense prediction tasks.

## REFERENCES

- [1] M. D. Zeiler and R. Fergus, “Visualizing and understanding convolutional networks,” in *Proc. European Conference on Computer Vision (ECCV)*. Springer, 2014, pp. 818–833.
- [2] J. Long, E. Shelhamer, and T. Darrell, “Fully convolutional networks for semantic segmentation,” in *Proc. IEEE Conference on Computer Vision and Pattern Recognition (CVPR)*, 2015, pp. 3431–3440.
- [3] V. Badrinarayanan, A. Kendall, and R. Cipolla, “SegNet: A deep convolutional encoder-decoder architecture for image segmentation,” *IEEE Transactions on Pattern Analysis and Machine Intelligence*, vol. 39, no. 12, pp. 2481–2495, 2017.
- [4] W. Shi, J. Caballero, F. Huszár, J. Totz, A. P. Aitken, R. Bishop, D. Rueckert, and Z. Wang, “Real-time single image and video super-resolution using an efficient sub-pixel convolutional neural network,” in *Proc. IEEE Conference on Computer Vision and Pattern Recognition (CVPR)*, 2016, pp. 1874–1883.
- [5] G. Lin, A. Milan, C. Shen, and I. Reid, “RefineNet: Multi-path refinement networks for high-resolution semantic segmentation,” in *Proc. IEEE Conference on Computer Vision and Pattern Recognition (CVPR)*, 2017, pp. 1925–1934.
- [6] L.-C. Chen, Y. Zhu, G. Papandreou, F. Schroff, and H. Adam, “Encoder-decoder with atrous separable convolution for semantic image segmentation,” in *Proc. European Conference on Computer Vision (ECCV)*, 2018.
- [7] N. Xu, B. Price, S. Cohen, and T. Huang, “Deep image matting,” in *Proc. IEEE Conference on Computer Vision and Pattern Recognition (CVPR)*, 2017, pp. 2970–2979.
- [8] T. Kraska, A. Beutel, E. H. Chi, J. Dean, and N. Polyzotis, “The case for learned index structures,” in *Proc. International Conference on Management of Data*. ACM, 2018, pp. 489–504.
- [9] M. Sandler, A. Howard, M. Zhu, A. Zhmoginov, and L.-C. Chen, “Mobilenetv2: Inverted residuals and linear bottlenecks,” in *Proc. IEEE Conference on Computer Vision and Pattern Recognition (CVPR)*, 2018, pp. 4510–4520.
- [10] K. Zhang, W. Zuo, Y. Chen, D. Meng, and L. Zhang, “Beyond a Gaussian denoiser: residual learning of deep CNN for image denoising,” *IEEE Transactions on Image Processing*, vol. 26, no. 7, pp. 3142–3155, 2017.
- [11] S. Roth and M. J. Black, “Fields of experts,” *International Journal of Computer Vision*, vol. 82, no. 2, p. 205, 2009.
- [12] S. Song, S. P. Lichtenberg, and J. Xiao, “SUN RGB-D: A RGB-D scene understanding benchmark suite,” in *Proc. IEEE Conference on Computer Vision and Pattern Recognition (CVPR)*, 2015, pp. 567–576.
- [13] N. Silberman, D. Hoiem, P. Kohli, and R. Fergus, “Indoor segmentation and support inference from rgb-d images,” in *Proc. European Conference on Computer Vision (ECCV)*. Springer, 2012, pp. 746–760.
- [14] H. Lu, Y. Dai, C. Shen, and S. Xu, “Indices matter: Learning to index for deep image matting,” in *Proc. IEEE/CVF International Conference on Computer Vision (ICCV)*, 2019.
- [15] A. Krizhevsky, I. Sutskever, and G. E. Hinton, “ImageNet classification with deep convolutional neural networks,” in *Advances in Neural Information Processing Systems (NIPS)*, 2012, pp. 1097–1105.
- [16] K. Simonyan and A. Zisserman, “Very deep convolutional networks for large-scale image recognition,” in *Proc. International Conference on Learning Representations (ICLR)*, 2014.
- [17] K. He, X. Zhang, S. Ren, and J. Sun, “Deep residual learning for image recognition,” in *Proc. IEEE conference on Computer Vision and Pattern Recognition (CVPR)*, 2016, pp. 770–778.
- [18] G. Huang, Z. Liu, L. Van Der Maaten, and K. Q. Weinberger, “Densely connected convolutional networks,” in *Proc. IEEE Conference on Computer Vision and Pattern Recognition (CVPR)*, 2017, pp. 4700–4708.

- [19] J. Hu, L. Shen, and G. Sun, "Squeeze-and-excitation networks," in *Proc. IEEE Conference on Computer Vision and Pattern Recognition*, 2018, pp. 7132–7141.
- [20] A. Odena, V. Dumoulin, and C. Olah, "Deconvolution and checkerboard artifacts," *Distill*, vol. 1, no. 10, p. e3, 2016.
- [21] C. Osendorfer, H. Soyer, and P. Van Der Smagt, "Image super-resolution with fast approximate convolutional sparse coding," in *Proc. International Conference on Neural Information Processing (ICONIP)*. Springer, 2014, pp. 250–257.
- [22] T.-J. Yang, M. D. Collins, Y. Zhu, J.-J. Hwang, T. Liu, X. Zhang, V. Sze, G. Papandreou, and L.-C. Chen, "DeeperLab: Single-shot image parser," *arXiv*, 2019.
- [23] M. Jaderberg, K. Simonyan, A. Zisserman *et al.*, "Spatial transformer networks," in *Advances in Neural Information Processing Systems (NIPS)*, 2015, pp. 2017–2025.
- [24] X. Jia, B. De Brabandere, T. Tuytelaars, and L. V. Gool, "Dynamic filter networks," in *Advances in Neural Information Processing Systems (NIPS)*, 2016, pp. 667–675.
- [25] J. Dai, H. Qi, Y. Xiong, Y. Li, G. Zhang, H. Hu, and Y. Wei, "Deformable convolutional networks," in *Proc. IEEE International Conference on Computer Vision (ICCV)*, 2017, pp. 764–773.
- [26] V. Mnih, N. Heess, A. Graves *et al.*, "Recurrent models of visual attention," in *Advances in Neural Information Processing Systems (NIPS)*, 2014, pp. 2204–2212.
- [27] F. Wang, M. Jiang, C. Qian, S. Yang, C. Li, H. Zhang, X. Wang, and X. Tang, "Residual attention network for image classification," in *Proc. IEEE Conference on Computer Vision and Pattern Recognition (CVPR)*, 2017, pp. 3156–3164.
- [28] S. Woo, J. Park, J.-Y. Lee, and I. So Kweon, "CBAM: Convolutional block attention module," in *Proc. European Conference on Computer Vision (ECCV)*, 2018, pp. 3–19.
- [29] Q. Chen, D. Li, and C.-K. Tang, "KNN matting," *IEEE Transactions on Pattern Analysis and Machine Intelligence*, vol. 35, no. 9, pp. 2175–2188, 2013.
- [30] Y.-Y. Chuang, B. Curless, D. H. Salesin, and R. Szeliski, "A bayesian approach to digital matting," in *Proc. IEEE Conference on Computer Vision and Pattern Recognition (CVPR)*. IEEE, 2001, p. 264.
- [31] K. He, C. Rhemann, C. Rother, X. Tang, and J. Sun, "A global sampling method for alpha matting," in *Proc. IEEE Conference on Computer Vision and Pattern Recognition (CVPR)*. IEEE, 2011, pp. 2049–2056.
- [32] A. Levin, D. Lischinski, and Y. Weiss, "A closed-form solution to natural image matting," *IEEE Transactions on Pattern Analysis and Machine Intelligence*, vol. 30, no. 2, pp. 228–242, 2008.
- [33] R. Girshick, J. Donahue, T. Darrell, and J. Malik, "Rich feature hierarchies for accurate object detection and semantic segmentation," in *Proc. IEEE Conference on Computer Vision and Pattern Recognition (CVPR)*, 2014, pp. 580–587.
- [34] D. Cho, Y.-W. Tai, and I. Kweon, "Natural image matting using deep convolutional neural networks," in *Proc. European Conference on Computer Vision (ECCV)*. Springer, 2016, pp. 626–643.
- [35] X. Shen, X. Tao, H. Gao, C. Zhou, and J. Jia, "Deep automatic portrait matting," in *Proc. European Conference on Computer Vision (ECCV)*. Springer, 2016, pp. 92–107.
- [36] T.-Y. Lin, M. Maire, S. Belongie, J. Hays, P. Perona, D. Ramanan, P. Dollár, and C. L. Zitnick, "Microsoft coco: Common objects in context," in *Proc. European Conference on Computer Vision (ECCV)*. Springer, 2014, pp. 740–755.
- [37] M. Everingham, L. Van Gool, C. K. Williams, J. Winn, and A. Zisserman, "The pascal visual object classes (voc) challenge," *International Journal of Computer Vision*, vol. 88, no. 2, pp. 303–338, 2010.
- [38] C. Rhemann, C. Rother, J. Wang, M. Gelautz, P. Kohli, and P. Rott, "A perceptually motivated online benchmark for image matting," in *Proc. IEEE Conference on Computer Vision and Pattern Recognition (CVPR)*. IEEE, 2009, pp. 1826–1833.
- [39] A. Paszke, S. Gross, S. Chintala, G. Chanan, E. Yang, Z. DeVito, Z. Lin, A. Desmaison, L. Antiga, and A. Lerer, "Automatic differentiation in pytorch," in *Advances in Neural Information Processing Systems Workshops (NIPSW)*, 2017.
- [40] J. Deng, W. Dong, R. Socher, L.-J. Li, K. Li, and L. Fei-Fei, "ImageNet: A large-scale hierarchical image database," in *Proc. IEEE Conference on Computer Vision and Pattern Recognition (CVPR)*. IEEE, 2009, pp. 248–255.
- [41] K. He, X. Zhang, S. Ren, and J. Sun, "Delving deep into rectifiers: Surpassing human-level performance on imagenet classification," in *Proc. IEEE International Conference on Computer Vision (ICCV)*, 2015, pp. 1026–1034.
- [42] D. P. Kingma and J. Ba, "Adam: A method for stochastic optimization," in *Proc. International Conference on Learning Representations (ICLR)*, 2015.
- [43] O. Ronneberger, P. Fischer, and T. Brox, "U-Net: Convolutional networks for biomedical image segmentation," in *Proc. International Conference on Medical Image Computing and Computer-Assisted Intervention (MICCAI)*. Springer, 2015, pp. 234–241.
- [44] C. Chen, Q. Chen, J. Xu, and V. Koltun, "Learning to see in the dark," in *Proc. IEEE Conference on Computer Vision and Pattern Recognition (CVPR)*, 2018, pp. 3291–3300.
- [45] R. Jaroensri, C. Biscarrat, M. Aittala, and F. Durand, "Generating training data for denoising real rgb images via camera pipeline simulation," *arXiv*, 2019.
- [46] K. Dabov, A. Foi, V. Katkovnik, and K. Egiazarian, "Image denoising by sparse 3-D transform-domain collaborative filtering," *IEEE Transactions on Image Processing*, vol. 16, no. 8, p. 2080, 2007.
- [47] H. C. Burger, C. J. Schuler, and S. Harmeling, "Image denoising: Can plain neural networks compete with BM3D?" in *IEEE Conference on Computer Vision and Pattern Recognition (CVPR)*. IEEE, 2012, pp. 2392–2399.
- [48] X. Mao, C. Shen, and Y.-B. Yang, "Image restoration using very deep convolutional encoder-decoder networks with symmetric skip connections," in *Advances in Neural Information Processing Systems (NIPS)*, 2016, pp. 2802–2810.
- [49] Y. Chen and T. Pock, "Trainable nonlinear reaction diffusion: A flexible framework for fast and effective image restoration," *IEEE Transactions on Pattern Analysis and Machine Intelligence*, vol. 39, no. 6, pp. 1256–1272, 2016.
- [50] L.-C. Chen, G. Papandreou, I. Kokkinos, K. Murphy, and A. L. Yuille, "DeepLab: Semantic image segmentation with deep convolutional nets, atrous convolution, and fully connected crfs," *IEEE Transactions on Pattern Analysis and Machine Intelligence*, vol. 40, no. 4, pp. 834–848, 2017.
- [51] H. Zhao, J. Shi, X. Qi, X. Wang, and J. Jia, "Pyramid scene parsing network," in *Proc. IEEE Conference on Computer Vision and Pattern Recognition (CVPR)*, 2017, pp. 2881–2890.
- [52] W. Liu, A. Rabinovich, and A. C. Berg, "ParseNet: Looking wider to see better," in *Proc. International Conference on Learning Representations (ICLR)*, 2015.
- [53] D. Eigen, C. Puhrsch, and R. Fergus, "Depth map prediction from a single image using a multi-scale deep network," in *Advances in Neural Information Processing Systems (NIPS)*, 2014, pp. 2366–2374.
- [54] F. Liu, C. Shen, G. Lin, and I. Reid, "Learning depth from single monocular images using deep convolutional neural fields," *IEEE Transactions on Pattern Analysis and Machine Intelligence*, vol. 38, no. 10, pp. 2024–2039, 2015.
- [55] C. Godard, O. Mac Aodha, and G. J. Brostow, "Unsupervised monocular depth estimation with left-right consistency," in *Proc. IEEE Conference on Computer Vision and Pattern Recognition (CVPR)*, 2017, pp. 270–279.
- [56] K. Xian, C. Shen, Z. Cao, H. Lu, Y. Xiao, R. Li, and Z. Luo, "Monocular relative depth perception with web stereo data supervision," in *Proc. IEEE Conference on Computer Vision and Pattern Recognition (CVPR)*, 2018, pp. 311–320.
- [57] D. Wofk, F. Ma, T.-J. Yang, S. Karaman, and V. Sze, "Fastdepth: Fast monocular depth estimation on embedded systems," in *Proc. IEEE International Conference on Robotics and Automation (ICRA)*, 2019.